Magnetoquantum oscillations of thermoelectric power in multisublevel quantum wires

S. K. Lyo
Sandia National Laboratories, Albuquerque, New Mexico 87185

Danhong Huang
Air Force Research Laboratory (AFRL/VSSS), Kirtland Air Force Base, New Mexico 87117

(Received 14 March 2002; revised manuscript received 13 June 2002; published 4 October 2002)

The electron-diffusion and phonon-drag thermoelectric power (TEP) is investigated in a quantum wire as a function of the temperature, perpendicular magnetic field, and the electron density in the regime, where the conductivity is limited by elastic scattering. The wire is narrow in the growth direction with only the ground sublevel populated but is wide in the other confinement direction providing several occupied sublevels at zero field. Magnetic field causes depopulation of these sublevels, yielding quantum oscillations of the TEP and the conductance. An anomalous, large positive electron-diffusion TEP is obtained when the Fermi level lies slightly above a sublevel other than the ground sublevel due to the van Hove singularity at the subband edge. In contrast to the power-law temperature (T) dependence in higher dimensions, the phonon-drag TEP is proportional to $\exp(-\hbar\omega_F/k_BT)$ at low temperatures, where $\hbar\omega_F$ is the threshold phonon energy with a wave number q_F corresponding to the minimum momentum transfer for back scattering.

DOI: 10.1103/PhysRevB.66.155307 PACS number(s): 73.63.Nm, 73.40.Kp, 72.20.Pa, 72.20.My

I. INTRODUCTION

Thermoelectric phenomena provide a powerful tool for investigating the electron and phonon transport dynamics and electron-phonon interaction. While a large amount of work has been devoted to the studies of the thermoelectric phenomena in the quasi-two-dimensional structures,[1–7] investigation of the phenomena in quasi-one-dimensional (1D) wires has attracted much less attention due to the difficulty in the sample growth.[8,9] Nevertheless, quasi-1D structures offer rich physics in the transport dynamics due to the restricted phase space and occupation of multisublevels with van Hove singularities at the bottom of the levels.[10,11] The quasi-1D structure of interest is shown in Fig. 1(a). The wire is along the y direction. In the z direction, only the ground level is relevant in this work due to the extreme confinement. However, the wire is wide in the x direction with several occupied sublevels. The ''sublevels'' in this paper designate these levels arising from the confinement in the x direction. The magnetic field B is in the z direction.

We are interested in the following features of the problem unique to the above system. The number of the occupied sublevels can be adjusted either by the electron density N_{1D} or by applying B. As is well known,[12] B increases the effective mass along the wire and therefore the density of states (DOS) for each sublevel. It also increases the sublevel separation. As B is increased under a fixed density, the sublevels pass through the chemical potential μ. The number of Fermi points changes as a function of B. Also, the DOS is a sensitive function of the energy, yielding a divergence at the bottom of each sublevel. Also, B displaces and localizes the wave functions in the x direction, affecting the interaction matrices. It is then expected that the thermoelectric power S will depend sensitively on N_{1D}, B, and the temperature T. Our theory predicts an anomalous, large positive electron-diffusion thermoelectric power (S_d) when the Fermi level lies slightly above the bottom of any of the sublevels above the ground sublevel. This is due to the fact that the conductance is very low at the energies near the bottom of a sublevel due to the 1D van Hove singularity and a small group velocity. As a result, more heat is carried by the quasiholes in the lower-energy sublevel(s). The phonon-drag thermoelectric power (S_{ph}) becomes large when many sublevels are occupied due to increased channels of electron-phonon scattering. S_{ph} is also sensitive to the threshold phonon energy $\hbar\omega_F$ with wave number $q=2k_F$ corresponding to the minimum momentum transfer for the scattering between the Fermi points in k space. As a result, $S_{ph}\propto\exp(-\hbar\omega_F/k_BT)$ has an exponential T-dependence at low T, in contrast to the well-known power-law behavior in higher dimensions. We consider bulk acoustic phonon modes interacting with the electrons through deformation and piezoelectric scattering.

The organization of the paper is as follows. In Sec. II, we introduce a parabolic potential model for the electronic states. This model yields analytic results and is employed for numerical applications and also for the purpose of elucidating the basic physical picture. A general formalism is presented for the conductance and S_{ph}, S_d in Secs. III and IV.

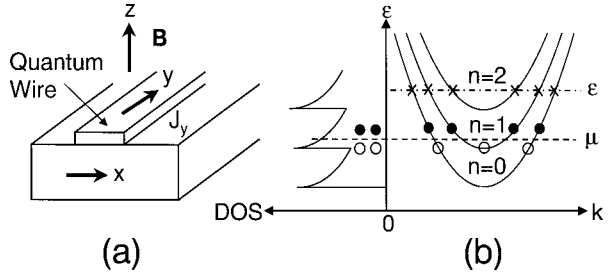

FIG. 1. Illustration of (a) a quasi-1D wire structure with an external perpendicular magnetic field B and (b) energy dispersion curves and the DOS for the first three sublevels. Solid and empty dots indicate quasiparticles and quasiholes near the chemical potential μ. The crosses signify the points in k space at energy ε for the sublevel dispersion curves.

Section III is devoted to the calculation of the electrical conductance in a magnetic field. The calculations of $S_{\rm ph}$ and $S_{\rm d}$ are presented in Sec. IV. In Sec. V, we present the analytic solutions for $S_{\rm ph}$ and $S_{\rm d}$ for a parabolic-well model. Numerical results and discussions are given in Sec. VI for the magnetic-field, temperature, and density dependence of $S_{\rm ph}$, $S_{\rm d}$, and the electrical conductance. The paper is concluded in Sec. VII.

II. FIELD-DEPENDENT ELECTRONIC STATES

We introduce a parabolic potential model to illustrate the effect of B on the electronic structure of the sublevels and for later numerical applications. The qualitative features of the results are expected to be independent of the model. The Hamiltonian for this model is given, for the motion in the x direction, by

$$\mathcal{H}_x = -\frac{\hbar^2}{2m^*}\frac{\partial^2}{\partial x^2} + \frac{1}{2}m^*\omega_x^2\, x^2, \tag{1}$$

where m^* is the effective mass of electrons and $\hbar\omega_x$ is the level separation of the harmonic eigen states. In the presence of $B||z$, the quantized electron energy relevant to the Hamiltonian in Eq. (1) is[10]

$$\varepsilon_j = \varepsilon_{n,k} = \left(n+\frac{1}{2}\right)\hbar\Omega_x + \frac{\hbar^2k^2}{2m^{**}}, \tag{2}$$

where k is the electron wave number along the wire, $m^{**} = m^*/[1-(\omega_{\rm c}/\Omega_x)^2]$, $\Omega_x = \sqrt{\omega_{\rm c}^2+\omega_x^2}$, $\omega_{\rm c} = eB/m^*c$, and $n = 0,1,2,\cdots$. The electrons are confined in the z direction by a rectangular well of width L_z and barrier height $U_{\rm c}$. Only the ground-state is assumed to be occupied in this direction. The Fermi wave number in the nth sublevel is $k_{n\rm F} = \sqrt{2m^{**}\varepsilon_{n\rm F}/\hbar}$, where $\varepsilon_{n\rm F}$ is the Fermi energy relative to the bottom of the sublevel.

The wave functions are given by[10]

$$\phi_{n,k}(x) = (\sqrt{\pi}2^n n! l_{cx})^{-1/2}\exp\left[-\frac{(x+\Delta x_k)^2}{2l_{cx}^2}\right]H_n\left(\frac{x+\Delta x_k}{l_{cx}}\right), \tag{3}$$

where $H_n(x)$ is the nth Hermite polynomial, $l_{cx} = \sqrt{\hbar c/m^*\Omega_x}$, $\Delta x_k = kl_{\rm c}^2(\omega_{\rm c}/\Omega_x)^2$, and $l_{\rm c} = \sqrt{\hbar c/eB}$. The total electron wave function of the quantum wire is given by

$$\psi_j(\mathbf{r}) = \frac{1}{\sqrt{L_y}}\exp(iky)\,\phi_{n,k}(x)\,\xi_0(z), \tag{4}$$

where $\xi_0(z)$ is the ground-state wave function in the z direction and L_y is the length of the wire. The energy and the wave function in the z direction are not affected by B. The wave functions in the x direction are displaced by the amount Δx_k due to the Lorentz force. The effective mass m^* of electrons is renormalized to m^{**}, significantly increasing the DOS with increasing B when the magnetic energy $\hbar\omega_{\rm c}$ becomes comparable to the confinement energy $\hbar\omega_x$. The energy-dispersion curves and the DOS are shown for the first three sublevels in Fig. 1(b). A very similar result can be obtained when B lies in the x direction if we assume a harmonic confinement in the z direction. In the present model, the effect of a magnetic field in the x direction is very small.

The physical picture which emerges from the above analysis is that the renormalized sublevel spacing $\hbar\Omega_x$ increases with B sensitively when the wire is wide in the x direction. Also, the effective electron mass m^{**} as well as the DOS increases with B. As a result, the sublevels $n = 1,2,\cdots$ pass through μ successively as B is increased. We show later that the position of μ with respect to the bottom of the sublevels affects $S_{\rm ph}$ and $S_{\rm d}$ as well as the conductance significantly.

III. NONEQUILIBRIUM ELECTRON-PHONON DISTRIBUTION FUNCTIONS

A. Linear deviation from equilibrium of the electron-phonon distributions

In this section, we present a formalism for the relationship between the nonequilibrium distribution functions of electrons and phonons coupled through electron-phonon interaction. We assume that the electron conduction is limited by elastic scattering such as impurity scattering or interface-roughness scattering at low temperatures. Inelastic scattering does not influence the electron current significantly at low temperatures.

Under the influence of an electric field E along the wire direction, the nonequilibrium electron distribution function is given to the first order in E by

$$f_j = f_0(\varepsilon_j) - f_0'(\varepsilon_j)\,\delta\mathcal{E}_j, \tag{5}$$

where $j=(n,k)$, $f_0(\varepsilon_j)$ is the Fermi function, and $f_0'(\varepsilon_j)$ is the first derivative with respect to the energy. The deviation function $\delta\mathcal{E}_j$ is linear in E. Similarly, the phonon distribution function is written as

$$n_{s\mathbf{q}} = n_0(\omega_{s,\mathbf{q}}) - n_0'(\omega_{s,\mathbf{q}})\,\delta\mathcal{W}_{s\mathbf{q}}, \tag{6}$$

where $n_0(\omega_{s,\mathbf{q}})$ is the Boson function and $n_0'(\omega_{s,\mathbf{q}})$ the first derivative with respect to $\hbar\omega_{s,\mathbf{q}}$. Here $\hbar\omega_{s,\mathbf{q}}$ is the energy of the phonon of mode s and wave vector $\mathbf{q}$.

The deviation function $\delta\mathcal{W}_{s\mathbf{q}}$ is induced through electron-phonon interaction and is linear in E. This quantity is related to the electron deviation function $\delta\mathcal{E}_j$ through the steady-state condition of the phonon distribution: $\dot{n}_{s\mathbf{q}}|_{scatt} + \dot{n}_{s\mathbf{q}}|_{pe} = 0$. Here, $\dot{n}_{s\mathbf{q}}|_{pe}$ and $\dot{n}_{s\mathbf{q}}|_{scatt}$ are the rates of the change of the phonon population through scattering from the electron-phonon interaction and other sources, respectively. For $\dot{n}_{s\mathbf{q}}|_{scatt}$, we assume a relaxation-time approximation:[13] $\dot{n}_{s\mathbf{q}}|_{scatt} = [n_0(\omega_{s,\mathbf{q}}) - n_{s\mathbf{q}}]/\tau_{s\mathbf{q}} = n_0'(\omega_{s,\mathbf{q}})\,\delta\mathcal{W}_{s\mathbf{q}}/\tau_{s\mathbf{q}}$, where the relaxation time $\tau_{s\mathbf{q}}$ of the phonons arises dominantly from the boundary scattering as will be discussed below. On the other hand, $\dot{n}_{s\mathbf{q}}|_{pe}$ is given by

$$\dot{n}_{s\mathbf{q}}|_{pe}=\frac{2\pi}{\hbar}\sum_{j,j'\pm}(\pm)|V^{s\mathbf{q}}_{j'j}|^2\, f_j(1-f_{j'})\left(n_{s\mathbf{q}}+\frac{1}{2}\pm\frac{1}{2}\right)\times\delta(\varepsilon'_j-\varepsilon_j\pm\hbar\omega_{s\mathbf{q}})\delta_{k',k\mp q_y}, \tag{7}$$

where $V^{s\mathbf{q}}_{j'j}$ is the electron-phonon interaction defined by $<n'k'|V^{\text{e-ph}}_{s,\mathbf{q}}|nk>=V^{s\mathbf{q}}_{j'j}\delta_{k',k+q_y}$ and the upper (lower) sign corresponds to the one-phonon emission (absorption) process except for the sign. Linearizing Eq. (7) according to Eqs. (5) and (6), using the steady-state condition we find, after a lengthy algebra,[4–6,14–16]

$$\delta\mathcal{W}_{s\mathbf{q}}=\left(\frac{2}{\tau^{-1}_{s\mathbf{q}}+a_{s\mathbf{q}}}\right)\frac{2\pi}{\hbar}\sum_{j,j'}|V^{s\mathbf{q}}_{j'j}|^2(\delta\mathcal{E}_{j'}-\delta\mathcal{E}_j)\times[f_0(\varepsilon_j)-f_0(\varepsilon_{j'})]\delta_{k',k+q_y}\delta(\varepsilon_j+\hbar\omega_{s,\mathbf{q}}-\varepsilon_{j'}), \tag{8}$$

where the spin degeneracy is included. The quantity

$$a_{s\mathbf{q}}=\frac{4\pi}{\hbar}\sum_{j,j'}|V^{s\mathbf{q}}_{j'j}|^2[f_0(\varepsilon_j)-f_0(\varepsilon_{j'})]\delta_{k',k+q_y}\times\delta(\varepsilon_j+\hbar\omega_{s,\mathbf{q}}-\varepsilon_{j'}) \tag{9}$$

in Eq. (8) originates from the linear term $\propto\delta\mathcal{W}_{s\mathbf{q}}$ contained in $n_{s\mathbf{q}}$ in Eq. (7) and indicates the contribution to the phonon relaxation rate via scattering by electrons. It is negligibly small compared with the contribution from boundary scattering in our structure due to the scarcity of the electrons and will be neglected.[1,2,16]

It was demonstrated earlier that a large number of 2D quantum wells (e.g., $\sim 10^3$) are necessary to compete with the boundary scattering at low temperatures.[16] The mean free path of a phonon due to the boundary scattering depends on the nature of the sample surface and is of the size of the sample dimension for absorbing (i.e., rough) boundaries. It can be increased by polishing the sample surface.[2,17] Since we are not comparing our results with any specific data in this paper, we assume absorbing boundaries and take the mean free path as a typical sample size, independent of the mode for a numerical evaluation, thereby estimating the lower limit of the phonon-drag thermopower. This kind of approximation was successfully employed previously to explain the phonon-drag thermopower in 2D quantum wells.[2,6]

B. Electron conductance

The electric conductance arises from the deviation function $\delta\mathcal{E}_j$ of the electron distribution, which is determined, at low temperatures, by elastic scattering through the Boltzmann equation

$$v_j+\frac{2\pi}{\hbar}\sum_{j'}|U_{j'j}|^2(g_{j'}-g_j)\delta(\varepsilon_j-\varepsilon_{j'})=0, \tag{10}$$

where $\delta\mathcal{E}_j=g_jeE$. Here, $v_j=\hbar^{-1}d\varepsilon_j/dk$ is the group velocity of electrons along the wire and $U_{j'j}$ is the elastic scattering matrix. The conductance was studied in detail recently by solving Eq. (10) exactly.[10] We summarize the important result in the following. The electrical current density is given by

$$J_y=G_{yy}\left(\frac{EL_y}{\mathcal{A}}\right)=\frac{2Ee^2}{h\mathcal{A}}\mathcal{G}, \tag{11}$$

where G_{yy} is the electrical conductance and

$$\mathcal{G}=-\int_0^{+\infty}d\varepsilon[-f'_0(\varepsilon)]\mathbf{s}^{\dagger}\underline{\mathbf{u}}^{-1}\mathbf{s}. \tag{12}$$

Here, $\mathcal{A}$ is the cross sectional area of the sample and $\underline{\mathbf{u}}^{-1}$ is the inverse of a nonsingular square matrix $\underline{\mathbf{u}}$ of rank $N_{\text{F}}-1$ with N_{F} being the number of points where the energy ε intersects the dispersion curves. These points are illustrated by the cross marks in Fig. 1(b) and will be designated as ''Fermi points'' since they are the Fermi points at $T=0$. These points are numbered $j=1,2,\cdots,N_{\text{F}}$ from the left to the right. The matrix $\underline{\mathbf{u}}$ is constructed from the $N_{\text{F}}\times N_{\text{F}}$ symmetric matrix:

$$u_{j,j'}=u_{j',j}=\frac{L_y}{\hbar^2}\frac{|U_{j'j}|^2}{|v_{j'}v_j|}\quad\text{for } j\neq j', \tag{13}$$

and

$$u_{j,j}=-\sum_{j'\neq j}u_{j,j'}, \tag{14}$$

by eliminating an arbitrary ith row and ith column. We will choose to eliminate the last point $i=N_{\text{F}}$ for convenience hereafter. The quantity $\mathbf{s}=\text{col}(s_1,s_2,s_3,\cdots,s_{N_{\text{F}}-1})$ in Eq. (12) is an $N_{\text{F}}-1$ dimensional column vector with its transpose $\mathbf{s}^{\dagger}$. The elements of $\mathbf{s}$ represent the signs $s_j=\pm1$ of the group velocity at the jth point. The original deviation function g_j is given, for $j=1,2,\cdots,N_{\text{F}}-1$, by

$$g_j=g'_j+g_{N_{\text{F}}},\quad \mathbf{g}'=-\underline{\mathbf{u}}^{-1}\mathbf{s}, \tag{15}$$

where $\mathbf{g}'=\text{col}(g'_1,g'_2,\cdots)$ is an $N_{\text{F}}-1$ dimensional column vector. The transport coefficients such as the conductance in Eq. (12) and S to be studied in Sec. IV depend only on $\mathbf{g}'$. The quantity $g_{N_{\text{F}}}$ is undetermined and irrelevant.[10] The phonon distribution function is determined from Eq. (8) using the relationship $\delta\mathcal{E}_j=g_jeE$ and depends only on $\mathbf{g}'$ in view of Eq. (15).

IV. THERMOELECTRIC POWER

A. Electron-diffusion thermoelectric power

The heat current density due to the electron diffusion is given, accounting for the spin degeneracy, by

$$Q_{\text{d}}=\frac{2eE}{\Omega}\sum_j v_jg_j\int_0^{\infty}d\varepsilon(\varepsilon-\mu)[-f'_0(\varepsilon)]\delta(\varepsilon_j-\varepsilon), \tag{16}$$

where $\Omega = L_y \mathcal{A}$ is the volume. The j summation includes summation on the sublevels and the energy integration over ε_{nk} with the DOS $\propto 1/|v_{nk}|$. This leads to

$$Q_{\rm d} = \frac{2eE}{Ah}\int_0^\infty d\varepsilon[-f_0'(\varepsilon)]\sum_{\nu=1}^{N_F} s_\nu g_\nu(\varepsilon_\nu - \mu) = \frac{2eE}{Ah}\int_0^\infty d\varepsilon[-f_0'(\varepsilon)]\sum_{\nu=1}^{N_F-1} s_\nu g_\nu'(\varepsilon_\nu - \mu), \quad (17)$$

where ε_ν is the energy at the νth Fermi point. The second equality follows from $g_\nu' = g_\nu - g_{N_F}$, $\Sigma_{\nu=1}^{N_F} s_\nu = 0$, and $\Sigma_{\nu=1}^{N_F} s_\nu \varepsilon_\nu = 0$. The electron-diffusion thermopower is then given by

$$S_{\rm d} = \frac{Q_{\rm d}}{J_y T} = \frac{1}{eT\mathcal{G}}\int_0^\infty d\varepsilon[-f_0'(\varepsilon)]\sum_{\nu=1}^{N_F-1} s_\nu g_\nu'(\varepsilon_\nu - \mu), \quad (18)$$

where $\mathcal{G}$ is defined in Eq. (12). The result in Eq. (18) reduces to Mott's formula $S_{\rm d} = (\pi^2 k_B^2 T/3e)\partial \ln \mathcal{G}/\partial\mu$ to the first order in T at extremely low temperatures. Here $\mathcal{G} = -\mathbf{s}^\dagger \underline{\mathbf{u}}^{-1}\mathbf{s}$ at $\varepsilon = \mu$.

B. Phonon-drag thermoelectric power

The heat current density due to phonon transport is given by

$$Q_{\rm ph} = \Omega^{-1}\sum_{s,\mathbf{q}} \hbar\omega_{s,\mathbf{q}}\, n_{s\mathbf{q}} \frac{\partial \omega_{s,\mathbf{q}}}{\partial q_y}. \quad (19)$$

Inserting Eqs. (6) and (8) into Eq. (19) and using the symmetry relations $\varepsilon_{n,-k} = \varepsilon_{n,k}$, $\omega_{s,-\mathbf{q}} = \omega_{s,\mathbf{q}}$, and $g_{n,-k} = -g_{n,k}$, we rewrite the heat current density in Eq. (19) as

$$Q_{\rm ph} = \sum_{j=1}^{N_{\rm F}} g_j Z_j, \quad (20)$$

where

$$Z_j = \frac{4\pi}{\hbar}\sum_{s,\mathbf{q},j';\pm} \frac{\partial \omega_{s\mathbf{q}}}{\partial q_y} F_{s,\mathbf{q}} |V_{j'j}^{s\mathbf{q}}|^2 [f_0(\varepsilon_j) - f_0(\varepsilon_{j'})] \times \delta_{k',k+q_y}(\pm)\,\delta(\varepsilon_{j'} \pm \hbar\omega_{s,\mathbf{q}} - \varepsilon_j) \quad (21)$$

and $F_{s,\mathbf{q}} = eE\tau_{s\mathbf{q}}\hbar\omega_{s,\mathbf{q}}[-n_0'(\omega_{s,\mathbf{q}})]/\Omega$. Using the antisymmetry relation $Z_{n,-k} = -Z_{n,k}$, we further reduce Eq. (20) to

$$Q = \sum_{j=1}^{N_{\rm F}-1} g_j' Z_j. \quad (22)$$

After employing the following identity

$$\mp[f_0(\varepsilon_{n,k}) - f_0(\varepsilon_{n',k+q_y})] = f_0(\varepsilon_{n,k})[1 - f_0(\varepsilon_{n',k+q_y})] \times \left[n_0(\omega_{s,\mathbf{q}}) + \frac{1}{2} \mp \frac{1}{2}\right]^{-1} \quad (23)$$

for $\varepsilon_{n',k+q_y} \pm \hbar\omega_{s,\mathbf{q}} - \varepsilon_{n,k} = 0$ in the expression in Eq. (21), we find the phonon-drag thermoelectric power from Eq. (22):

$$S_{\rm ph} = \frac{Q}{J_y T} = -\left[\frac{k_B \mathcal{A}h}{e\Omega(k_B T)^2 \mathcal{G}}\right]\frac{2\pi}{\hbar}\sum_{s,\mathbf{q};\pm} \hbar\omega_{s,\mathbf{q}} \frac{\partial \omega_{s,\mathbf{q}}}{\partial q_y}\tau_{s\mathbf{q}} \times \left[n_0(\omega_{s,\mathbf{q}}) + \frac{1}{2} \pm \frac{1}{2}\right] \times \sum_{n,n';k} g_{n,k}' f_0(\varepsilon_{n,k}) \times [1 - f_0(\varepsilon_{n',k+q_y})]|V_{n'n}^{s\mathbf{q}}|^2 \times \delta(\varepsilon_{n',k+q_y} \pm \hbar\omega_{s,\mathbf{q}} - \varepsilon_{n,k}). \quad (24)$$

It is important to note that G_{yy}, $S_{\rm d}$, and $S_{\rm ph}$ depend only on $N_{\rm F}$-1-dimensional $\mathbf{g}'$ instead of $N_{\rm F}$-dimensional $\mathbf{g}$. The formalism derived in this section for S and the conductance is general for any 1D system.

V. PARABOLIC QUANTUM WIRE

In this section, we apply the results to the structure where the confinement in the x direction is due to a parabolic potential, studied in Sec. II.

In the parabolic quantum-wire model, the quantity $|V_{n'n}^{s\mathbf{q}}|^2$ in Eq. (24) is given by

$$|V_{n'n}^{s\mathbf{q}}|^2 = (V_{s\mathbf{q}}^2/\epsilon_n\epsilon_{n'})\Delta_{n'n}(q_x,q_y)\Delta_z(q_z), \quad (25)$$

where

$$\Delta_{n'n}(q_x,q_y) = \frac{n_<!}{n_>!}P^m \exp(-P)[L_{n_<}^m(P)]^2, \quad (26)$$

$P = [(\Delta x_{q_y})^2 + q_x^2 l_{cx}^4]/2l_{cx}^2$, $m = n_> - n_<$, and $n_>$ ($n_<$) are the larger (lesser) of n and n'. In Eq. (26), $L_n^m(x)$ is the associated Laguerre polynomial. $\Delta_z(q_z)$ in Eq. (25) is

$$\Delta_z(q_z) = \left|\int_{-\infty}^{+\infty} dz \exp(iq_z z)|\xi_0(z)|^2\right|^2. \quad (27)$$

For the longitudinal ($s = l$) and transverse ($s = t$) modes of acoustic phonons, the quantity $V_{s\mathbf{q}}^2$ introduced in Eq. (25) is

$$V_{l\mathbf{q}}^2 = \frac{\hbar\omega_{l\mathbf{q}}}{2\Omega\rho_{\rm mass}c_l^2}\left[D^2 + (eh_{14})^2\frac{A_l(\mathbf{q})}{q^2}\right], \quad (28)$$

$$V_{t\mathbf{q}}^2 = \frac{\hbar\omega_{t\mathbf{q}}}{2\Omega\rho_{\rm mass}c_t^2}(eh_{14})^2\frac{A_t(\mathbf{q})}{q^2}, \quad (29)$$

where $\rho_{\rm mass}$, c_s, D, and h_{14} are the mass density, sound velocity, deformation-potential coefficient, and piezoelectric constant.[5] The quantities $A_s(\mathbf{q})$ in Eqs. (28) and (29) are given by[18]

$$A_l(\mathbf{q})=\frac{36q_x^2q_y^2q_z^2}{q^6},$$

$$A_t(\mathbf{q})=\frac{2[q^2(q_x^2q_y^2+q_y^2q_z^2+q_z^2q_x^2)-9q_x^2q_y^2q_z^2]}{q^6}. \quad (30)$$

In Eq. (25), ϵ_n^{-1} is given by $[\epsilon^{-1}(q_y)]_{n,n}$ in the static Thomas-Fermi (TF) approximation. Here the matrix elements of the dielectric functions ϵ are[19,20]

$$\epsilon_{n,n'}(q_y)=\delta_{n,n'}+q_n^{\mathrm{TF}}F_{nn'}(q_y), \quad (31)$$

where the inverse TF screening length is

$$q_n^{\mathrm{TF}}=\left(\frac{2e^2}{k_BT\kappa}\right)\int_0^{+\infty}d\varepsilon_{n,k}\left[\hbar|v_{n,k}|\cosh^2\left(\frac{\varepsilon_{n,k}-\mu(T)}{2k_BT}\right)\right]^{-1}, \quad (32)$$

and the form factor due to finite-size quantization is

$$\begin{aligned}F_{n,n'}(q_y)=&\frac{1}{2\pi}\int_{-\infty}^{+\infty}dx\int_{-\infty}^{+\infty}dx'\int_{-\infty}^{+\infty}dz\\&\times\int_{-\infty}^{+\infty}dz'|\phi_{n,0}(x)|^2|\phi_{n',0}(x')|^2\\&\times|\xi_0(z)|^2|\xi_0(z')|^2\\&\times K_0(|q_y|\sqrt{(x-x'+\Delta x_{q_y})^2+(z-z')^2}).\end{aligned} \quad (33)$$

Here, $K_0(x)$ is the modified Bessel function and κ in Eq. (33) is the bulk dielectric constant. The expression in Eq. (32) reduces to $q_n^{\mathrm{TF}}=8e^2/\hbar v_{0\mathrm{F}}\kappa\equiv q_0$ in the limit $k_BT\ll\varepsilon_{0\mathrm{F}}$. For single-sublevel occupation $n=0$, q_n^{TF} in Eq. (32) is the limiting expression (i.e., $q_y\to 0$) of the RPA (random phase approximation) result q_n^{RPA}.[21] The RPA expression has a well-known logarithmic singularity for $q_y=\pm 2k_{\mathrm{F}}$ scattering at $T=0$. In the limit $k_BT\ll\varepsilon_{0\mathrm{F}}$, the RPA yields

$$q_0^{\mathrm{RPA}}=\frac{1}{2}q_0[\ln(\varepsilon_{0\mathrm{F}}/k_BT)+1.512] \quad (34)$$

for $q_y=\pm 2k_{\mathrm{F}}$.

We now carry out the integrations over k and $\mathbf{q}$ in Eq. (24). For this purpose, it is convenient to introduce the following identity between the Fermi-Dirac distribution $f_0(x)$ and the Bose-Einstein distribution $n_0(z)$:

$$\begin{aligned}f_0(x)[1-f_0(y)]\delta(x+z-y)=&z\left[\frac{f_0(x)-f_0(y)}{z}\right]\\&\times[1+n_0(z)]\delta(x+z-y).\end{aligned} \quad (35)$$

At low temperatures, the right-hand side of this identity can be approximated for small z as[4]

$$\begin{aligned}&f_0(x)[1-f_0(y)]\delta(x+z-y)\\&\quad\approx z[1+n_0(z)]\delta(x-\mu)\delta(x-y).\end{aligned} \quad (36)$$

Inserting $x=\varepsilon_{n,k}, y=\varepsilon_{n',k'}$ into Eq. (36), using $z=-\hbar\omega_{s,\mathbf{q}}$ for the upper sign and $z=\hbar\omega_{s,\mathbf{q}}$ for the lower sign in Eq. (24), and carrying out the integration over k and $\mathbf{q}$, we find

$$S_{\mathrm{ph}}=\int_0^{+\infty}d\varepsilon[-f_0'(\varepsilon)]\mathcal{D}(\varepsilon). \quad (37)$$

where

$$\begin{aligned}\mathcal{D}(\varepsilon)=&-\left[\frac{8k_B/e}{(2\pi k_BT)^2\mathcal{G}\hbar^2}\right]\int_0^{+\infty}dq_x\int_0^{+\infty}dq_z\\&\times\sum_s(\hbar\omega_{s,\mathbf{q}})^2\frac{q_y}{q}\Lambda_{s\mathbf{q}}\sum_{j=1}^{N_{\mathrm{F}}-1}\sum_{j'=1}^{N_{\mathrm{F}}}n_0(\omega_{s,\mathbf{q}})[n_0(\omega_{s,\mathbf{q}})\\&+1]g_j'\Omega|V_{j'j}^{s\mathbf{q}}|^2\frac{1}{|v_jv_{j'}|}\delta_{q_y,k'-k}.\end{aligned} \quad (38)$$

Here $j=(n,k)$ represents the states at the intersection of the energy ε and the dispersion curves. In Eq. (38), the Debye approximation is employed for the long-wavelength phonons $\omega_{s,\mathbf{q}}=c_sq$ and $\Lambda_{s\mathbf{q}}=c_s\tau_{s\mathbf{q}}$ is the phonon mean free path. The wave numbers k,k' in Eq. (38) at points j,j' are given by

$$k=-\frac{q_y}{2}+\frac{\mp\hbar\omega_{s,\mathbf{q}}+(n-n')\hbar\Omega_x}{\hbar^2q_y/m^{**}},$$

$$k'=\frac{q_y}{2}+\frac{\mp\hbar\omega_{s,\mathbf{q}}+(n-n')\hbar\Omega_x}{\hbar^2q_y/m^{**}}. \quad (39)$$

The divergence at $v_j=0$ in Eqs. (32) and (38) at the bottom of the sublevels is avoided by introducing a level-broadening parameter γ_j at the bottom of the subband for the jth Fermi point[10]

$$\frac{1}{v_j}=\begin{cases}(m^{**}/\gamma_j)^{1/2} & \text{if } 1/v_j>(m^{**}/\gamma_j)^{1/2}\\ 1/v_j & \text{if } 1/v_j\leqslant(m^{**}/\gamma_j)^{1/2}.\end{cases} \quad (40)$$

VI. NUMERICAL RESULTS AND DISCUSSIONS

In our numerical calculations, we study a GaAs wire imbedded in AlGaAs and assume: $L_z=100$ Å (quantum-well width), $U_c=280$ meV (barrier height), $m_B=0.073\ m_0$ (mass in the barrier with free-electron mass m_0), $\kappa=12$, $m^*=0.067\ m_0$, $c_l=5.14\times10^5$ cm/sec, $c_t=3.04\times10^5$ cm/sec, $\rho_{\mathrm{mass}}=5.3$ g/cm^3, $h_{14}=1.2\times10^7$ V/cm, $D=-9.3$ eV, $\Lambda_{s\mathbf{q}}=0.3$ mm, and $\gamma_j=0.16$ meV.[5,6,10] We also assume that elastic scattering for the conductance is dominated by the interface-roughness of a monolayer fluctuation $\delta b=5$ Å with a correlation length given by $\Lambda_x=\Lambda_y=30$ Å as studied earlier.[10] Other parameters will be given in the corresponding figure captions.

We plot in Fig. 2(a) the T dependence of the thermopower at $B=0$ for $\hbar\omega_x=50$ meV and $N_{1\mathrm{D}}=1\times10^6$ cm^{-1}, where

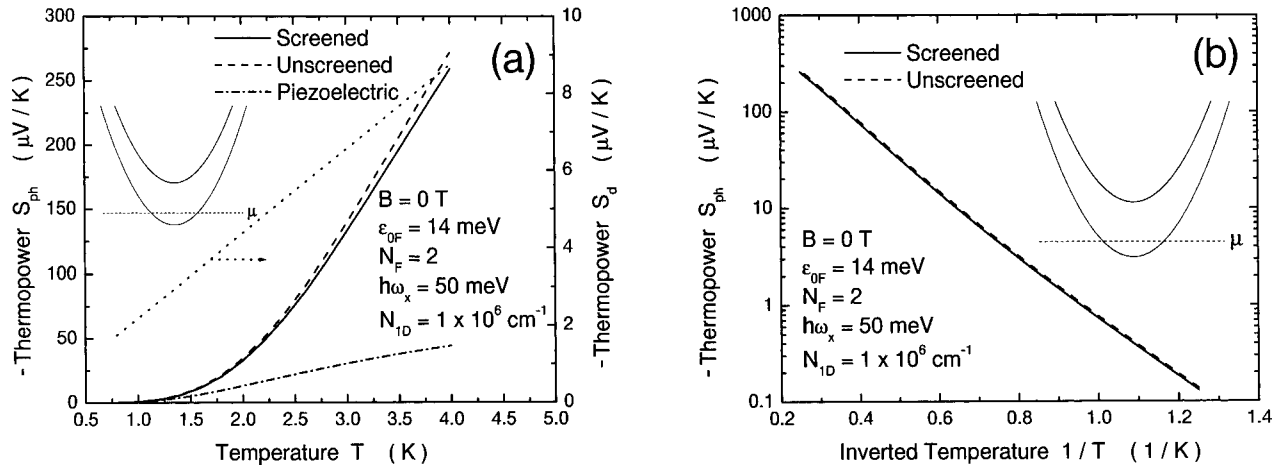

FIG. 2. (a) Phonon-drag ($S_{\rm ph}$, solid, dashed curves, left axis) and electron-diffusion ($S_{\rm d}$, dotted curve, right axis) thermopower as a function of the temperature T at $B=0$. Only the first sublevel $n=0$ is populated (i.e., $N_{\rm F}=2$) with the Fermi energy $\varepsilon_{0\rm F}=14$ meV. The dash-dotted curve represents the contribution to $S_{\rm ph}$ from the screened piezoelectric interaction. (b) Semilog plot of the phonon-drag thermopower vs $1/T$. The activation energy corresponds to the transverse acoustic phonon energy with $q_y=2k_{0\rm F}$.

only the lowest sublevel ($n=0$) is occupied with $\varepsilon_{0\rm F}=14$ meV and $N_{\rm F}=2$. The effect of smaller $\hbar\omega_x=10$ and 1 meV will be studied later. The phonon-drag contribution $S_{\rm ph}$ in Fig. 2(a) shows a typical 3D T^3 dependence around 3 K due to the ω^2-dependent bulk phonon DOS and rises with a smaller exponent above 3 K due to the x and z confinement. A similar result was obtained earlier.[8] On the other hand, $S_{\rm ph}$ decreases rapidly as $\exp(-\hbar\omega_{\rm F}/k_BT)$ for decreasing T below 2 K as shown in Fig. 2(b). Here $\hbar\omega_{\rm F}$ is approximately the minimum phonon energy necessary to scatter an electron across the Fermi surface, namely the transverse phonon energy corresponding to the wave number $q_y=2k_{0\rm F}$. This activation behavior is unique to a one-dimensional structure where the Fermi surface consists of two discrete points. We have also considered ''vertical'' phonon scattering processes around each Fermi point corresponding to $j=j'$ in Eq. (38). This contribution arises from the small-q_y solution in Eq. (39) with $n=n'$, namely $q_y\simeq\mp k\hbar\omega_{s,\mathbf{q}}/2\varepsilon_{0\rm F}-k(\hbar\omega_{s,\mathbf{q}}/\varepsilon_{0\rm F})^2/8$ for the absorption and emission processes. Here it is clear that the first term cancels out for one-phonon emission and absorption processes, leaving only the second term $q_y\sim-k(k_BT/\varepsilon_{0\rm F})^2/8$, which is very small (i.e., $k_BT/\varepsilon_{0\rm F}\ll1$). Although this contribution yields a power-law T dependence and dominates the above exponential $S_{\rm ph}$ for $T\to0$, it is still about three orders of magnitude smaller than $S_{\rm ph}$ shown in Fig. 2 at $T=0.8$ K and is negligible in the range of T shown there. This arises from the fact that $\hbar\omega_{\rm F}/\varepsilon_{0\rm F}\ll1$. In the low temperature range $T\leqslant1.5$ K shown in Fig. 2(a), the main contribution to $S_{\rm ph}$ arises from the piezoelectric interaction with long-wavelength phonons as shown by the dash-dotted curve. The electron-diffusion contribution $S_{\rm d}$ in Fig. 2(a) is linear in T, becomes larger than $S_{\rm ph}$ in magnitude below 1.2 K and deviates from the linear behavior at high T.

In Fig. 3, we examine the accuracy of $S_{\rm ph}$ based on the TF approximation (dashed curve) by comparing it with that obtained from the RPA (solid curve). At low temperatures, the effect of damping ($\Gamma\gg k_BT$) is expected to be important. The damping effect on the inverse screening length is calculated from the result of Das Sarma and Lai[22] for $k_BT\ll\varepsilon_{0\rm F}$ and is shown in the inset. For the ratio $\alpha\equiv\Gamma/\varepsilon_{0\rm F}=0.1$ employed for the solid curve for $S_{\rm ph}$, $q_{\rm RPA}\simeq4q_0$ at $q_y=\pm2k_{0\rm F}$ is larger than $q_0^{\rm RPA}$ in Eq. (34) in the temperature range shown in Fig. 3. It is seen that the TF approximation overestimates $|S_{\rm ph}|$ by less than 10% compared with the RPA. For multilevel occupation, the most important effect occurs when μ is slightly above the bottom of a sublevel, where α is close to unity. In this case, screening is dominated by this level due to the large DOS near μ. Therefore, the TF approximation is expected to give a similar result to that of the RPA because $q_{\rm RPA}\sim q_o$ for $q_y=\pm2k_{0\rm F}$ as seen from the inset.

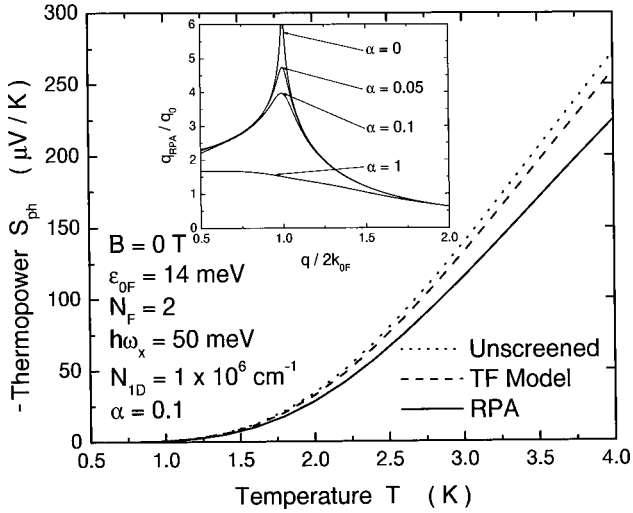

FIG. 3. Comparison of S_{ph} due to TF approximation with that from the RPA. The ratio $q_{\rm RPA}/q_0$ of the inverse RPA screening length to that from TF approximation is obtained in the low-T $\ll\varepsilon_{0\rm F}k_B^{-1}$ limit and is displayed in the inset for several values of $\alpha=\Gamma/\varepsilon_{0\rm F}$.

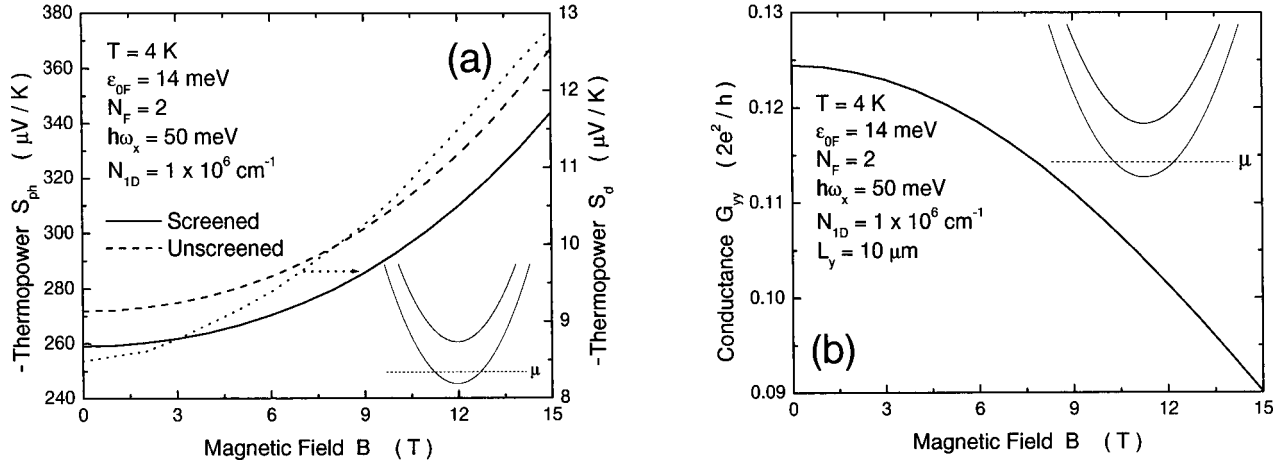

FIG. 4. B dependence of (a) $S_{\rm ph}$ (solid, dashed curves, left axis) and $S_{\rm d}$ (dotted curve, right axis) and (b) G_{yy} (solid curve) at $T=4$ K. Only the ground sublevel is populated ($N_{\rm F}=2$) for this sample.

Figure 4(a) displays $S_{\rm ph}$ and $S_{\rm d}$ as a function of B at $T=4$ K for the same sample parameters as in Fig. 2. The dielectric screening reduces $S_{\rm ph}$ significantly. The quadratic B dependence of $S_{\rm ph}$ is a consequence of the B-enhancement of the DOS $\propto\sqrt{m^{**}}$. The B dependence enters Eqs. (37) and (38) for $S_{\rm ph}$ in three ways. One is the product $1/|v_j v_{j'}|$, namely the product of the DOS at the Fermi points j and j'. The second is the overlap factor $\Delta_{n'n}(q_x, q_y)$ introduced in Eqs. (25) and (26) for the electron-phonon interaction. This factor decreases for increasing B due to the B-induced displacement of the wave functions. This effect is important only at high B. The third factor is the phonon occupation number $n_0(\omega_{s,\mathbf{q}})$, where the minimum phonon energy is restricted by $q_y=2k_{0\rm F}$. In this regard, the q-dependence of $V^2_{s\mathbf{q}}\propto q, q^{-1}$ in the deformation-potential and piezoelectric scattering also affects $S_{\rm ph}$. In the present case of single-level occupation, $k_{0\rm F}$ is independent of B due to the conservation of the number of the electrons. For the case of multilevel occupation, it can depend sensitively on B through the DOS. The quantity $S_{\rm d}$ (dotted curve with right scale) also rises quadratically with B. The origin of this behavior has the following explanation. The contribution to the conductance from a given energy level ε is $G\propto v^2\rho\tau$, where v is the group velocity, $\rho\propto|v|^{-1}$ is the DOS, and $\tau\propto\rho^{-1}$ is the scattering time. Therefore $G\propto\rho^{-2}\propto\varepsilon$ is a decreasing function of the DOS and is larger for the quasiparticles than the quasiholes, yielding a negative $S_{\rm d}$. The absolute value of $S_{\rm d}$ is given by $|S_{\rm d}|\propto G^{-1}\partial G/\partial\varepsilon\propto\varepsilon^{-1}$ and increases as $\propto\varepsilon^{-1}=2m^{**}/(\hbar k_{0\rm F})^2\propto m^{**}\simeq m^*(1+\omega_c^2/\omega_x^2)$ as a function of B. The B-dependent behavior of $G=G_{yy}$ can be explained similarly.

If the electron density $N_{\rm 1D}$ is lowered to 0.5×10^6 cm^{-1} with the other parameters in Fig. 4 fixed, both $S_{\rm ph}$ and $S_{\rm d}$ increase dramatically as shown in Fig. 5(a). In this case, both the phonon population for $q_y=2k_{0\rm F}=\pi N_{\rm 1D}$ and the DOS $\propto 1/N_{\rm 1D}$ at the Fermi level increase significantly. Contrary to this, G_{yy} (solid curve) reduces with $N_{\rm 1D}$ due to the larger DOS or the lower Fermi velocity, as shown in Fig. 5(b).

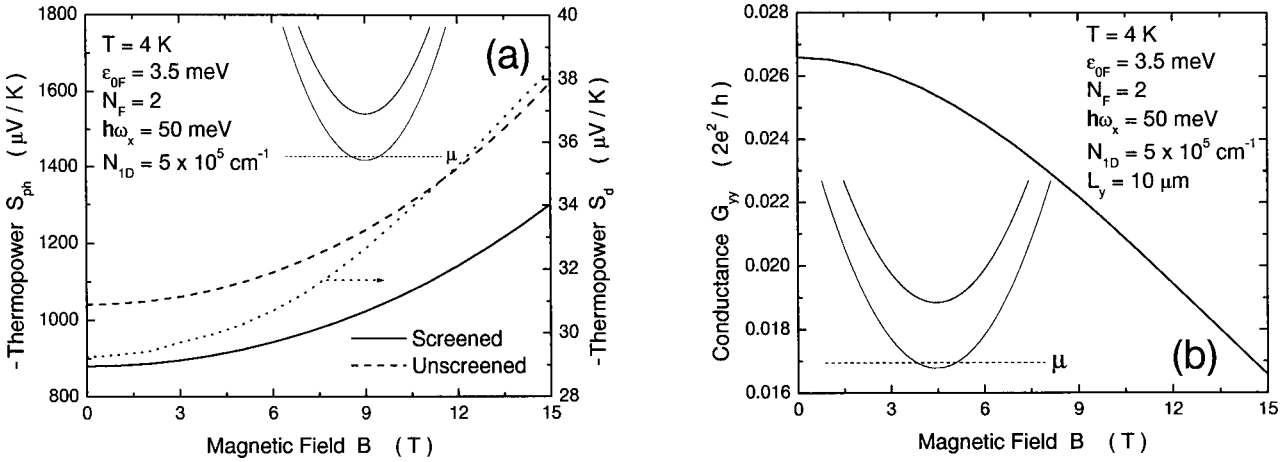

FIG. 5. B dependence of (a) $S_{\rm ph}$ (solid, dashed curves, left axis) and $S_{\rm d}$ (dotted curve, right axis) and (b) G_{yy} at $T=4$ K for $\hbar\omega_x=50$ meV, $N_{\rm 1D}=0.5\times10^6$ cm^{-1}, and $L_y=10$ μm (for G_{yy}). Only the $n=0$ sublevel is occupied (i.e., $N_{\rm F}=2$) with $\varepsilon_{0\rm F}=3.5$ meV. Other parameters are given in the text.

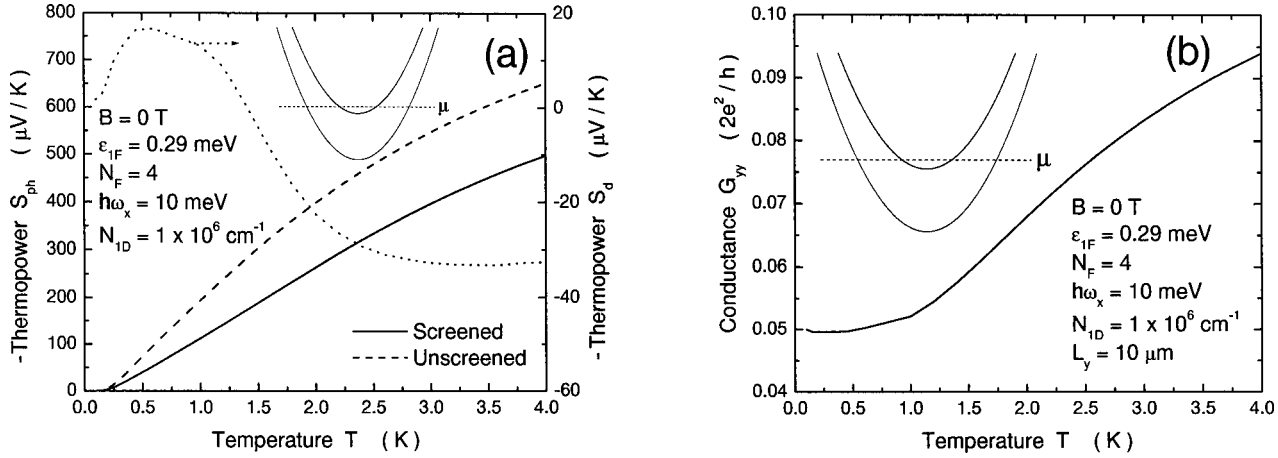

FIG. 6. T dependence of (a) $S_{\rm ph}$ (solid, dashed curves, left axis) and $S_{\rm d}$ (dotted curve, right axis) and (b) G_{yy} for $L_y=10$ μm at $B=0$ for two-sublevel occupation $N_{\rm F}=4$. Other parameters are given in the text.

The discussions so far have been limited to the extreme quantum limit where only the ground sublevel $n=0$ is populated. We now study the situation where $\hbar\omega_x$ is reduced to 10 meV with the same $N_{\rm 1D}=10^6$ cm^{-1} studied in Figs. 2 and 4. In this case, the second sublevel $n=1$ is populated near the bottom with a small Fermi energy $\varepsilon_{\rm 1F}=0.29$ meV. The T dependence of $S_{\rm ph}$ (solid, dashed curves, left scale) and $S_{\rm d}$ (dotted curve, right scale) is shown at $B=0$ in Fig. 6(a). The exponential T-dependence for $S_{\rm ph}$ is seen only at extremely low $T<0.25$ K because $q=2k_{\rm 1F}$ is small. The quantity $-S_{\rm d}$ rises linearly below 0.15 K and more steeply between 0.15 K$<T<$0.5 K with a negative sign for $S_{\rm d}$ and then decreases rapidly. What is striking, however, is that $S_{\rm d}$ changes sign, yielding a positive value. Its magnitude is larger than the screened $|S_{\rm ph}|$ below 0.27 K. A positive sign for $S_{\rm d}$ from the electron heat transport is unusual and has the following explanation: Due to the proximity of μ to the bottom of the sublevel $n=1$, the DOS near the thermal layer is very large above μ for the quasiparticles with a small G and small for the quasiholes in the sublevel $n=0$ below μ with a large G. Therefore, the heat is carried mainly by the quasiholes, yielding a positive $S_{\rm d}$. The conductance displayed in Fig. 6(b) increases with T because the current is more efficiently carried by the quasiholes and particles away from the large-DOS region.

We display the $N_{\rm 1D}$ dependence of $S_{\rm ph}$ (solid, dashed curves, left scale), $S_{\rm d}$ (dotted curve, right scale), and G_{yy} in Fig. 7 at $T=2$ K and $B=0$ for $\hbar\omega_x=10$ meV. The vertical arrows indicate the density $N_{\rm 1D}=0.92\times10^6$ cm^{-1} where the second sublevel begins to be populated. The quantity $q_y=2k_{\rm 0F}$ reaches its maximum value just before the thermal occupation of the $n=1$ sublevel, yielding the minimum in $-S_{\rm ph}$ around $N_{\rm 1D}=0.8\times10^6$ cm^{-1} as discussed earlier. The quantity $q_y=2k_{\rm 1F}$ becomes small just above the arrow and increases with $N_{\rm 1D}$, yielding a sharp peak in $-S_{\rm ph}$ around $N_{\rm 1D}=1.02\times10^6$ cm^{-1} as shown in Fig. 7(a). This sharp minimum-maximum structure is rounded at higher temperatures. $S_{\rm d}$ undergoes a sign change to a positive value and becomes large between the dip and peak of $-S_{\rm ph}$. It is interesting to note that $S_{\rm d}$ nearly cancels out $S_{\rm ph}$ near $N_{\rm 1D}=0.9\times10^6$ cm^{-1}. A similar level depopulation can be cre-

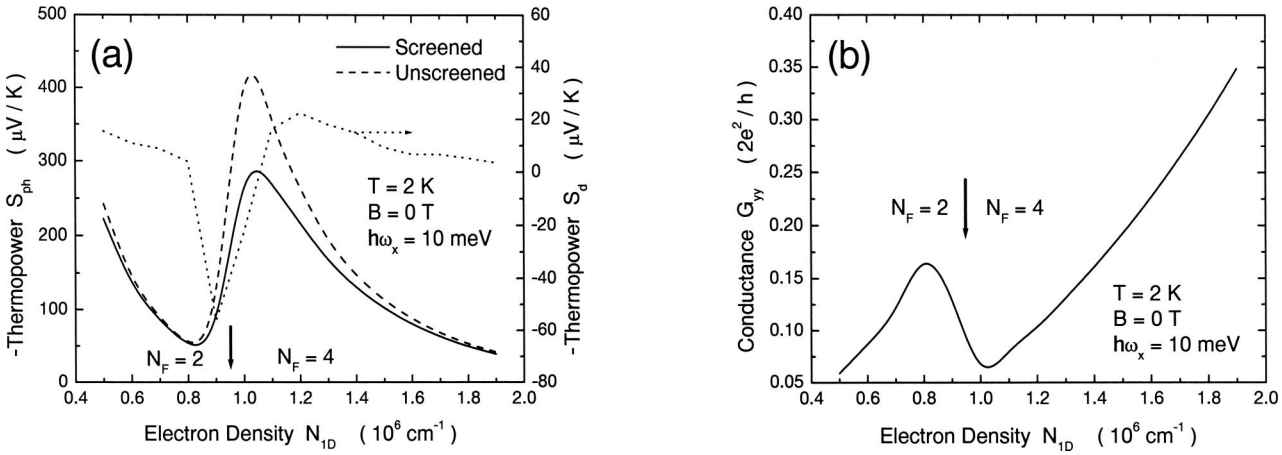

FIG. 7. $N_{\rm 1D}$ dependence of (a) $S_{\rm ph}$ (solid, dashed curves, left axis) and $S_{\rm d}$ (dotted curve, right axis) and (b) G_{yy} at $T=2$ K and $B=0$ for $\hbar\omega_x=10$ meV and $L_y=10$ μm (for G_{yy}). Other parameters are given in the text. The vertical arrows in (a) and (b) indicate $N_{\rm 1D}$ where the second sublevel begins to be populated.

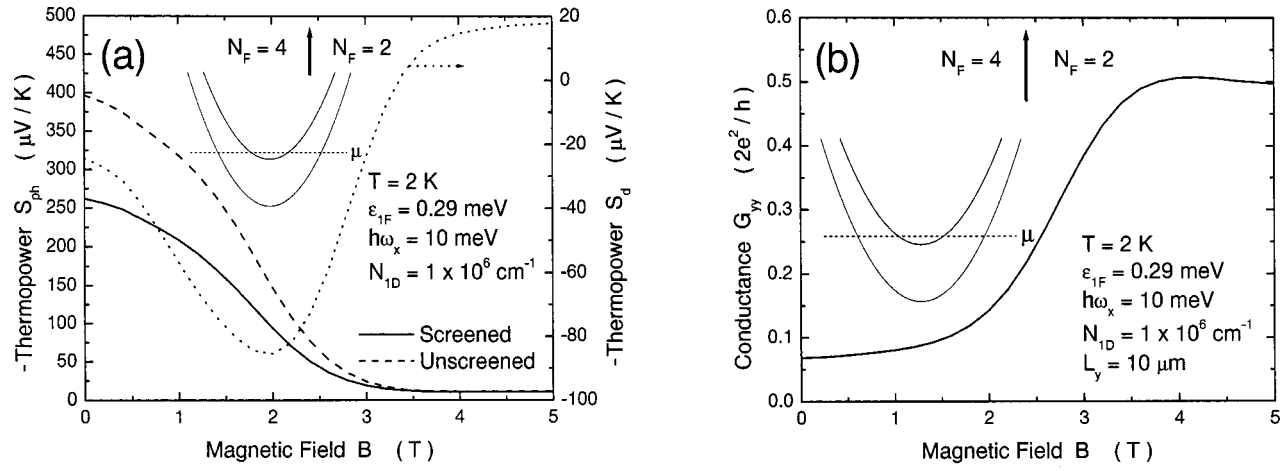

FIG. 8. B dependence of (a) $S_{\rm ph}$ (solid, dashed curves, left axis) and $S_{\rm d}$ (dotted curve, right axis) and (b) G_{yy} at $T=2$ K for $\hbar\omega_x=10$ meV, $N_{1D}=1\times10^6$ cm^{-1}, $L_y=10$ μm (for G_{yy}). Other parameters are given in the text. Two sublevels are populated at $B=0$ with $\varepsilon_{1F}=0.29$ meV and $N_F=4$. The vertical arrows in (a) and (b) indicate the magnetic field at which the second sublevel is depopulated.

ated by a magnetic field as will be shown in Fig. 8. The conductance G_{yy} in Fig. 7(b) has a peak and a dip just below and above the arrow near the minimum and maximum of the total DOS, respectively. This behavior can readily be under stood from the argument $G\propto\rho^{-2}$ presented for Fig. 4 earlier in this section. A much shallower dip is expected in two dimensions due to the absence of the van Hove singularity as has been observed.[23]

In the rest of the section, we discuss the B-dependence and the effect of multisublevel occupation on $S_{\rm ph}$,$S_{\rm d}$, and G_{yy}. In Fig. 8, we study the sample with $\hbar\omega_x=10$ mev and $N_{1D}=10^6$ cm^{-1}, which was studied in Fig. 6. Here, the Fermi level is near the bottom of the $n=1$ sublevel. In Fig. 8(a), $-S_{\rm ph}$ decreases rapidly with B because the $n=1$ sublevel is depopulated near $B=2.4$ T (marked by a vertical arrow). In this case, $\varepsilon_{1F}=0.29$ meV is close to the level broadening $\gamma_j=0.16$ meV. Here, $q_y=2k_{1F}$ is already small at $B=0$ and $n_0(\omega_{s,\mathbf{q}})$ is not the major source of the B dependence because $\hbar\omega_{s,\mathbf{q}}\lesssim k_BT$ at $T=2$ K. This is not true at low temperatures where an opposite B-dependent behavior is found for $S_{\rm ph}$ at $T=0.2$ K as will be studied in Fig. 9. The situation in Fig. 8 at $B=0$ is very similar to that studied in Fig. 7 near the level depopulation density N_{1D} indicated by the arrow and can be explained using the same physics. As B increases, the chemical potential falls below the sublevel $n=1$, pushing $-S_{\rm ph}$ toward the minimum. In the present case, however, $-S_{\rm ph}$ continues to decrease monotonically due to the overlap factor $\Delta_{n'n}(q_x,q_y)$ in Eqs. (25) and (26) as discussed earlier. The mechanism of the sign change of $S_{\rm d}$ in Fig. 8(a) as well as the large anomalous positive $S_{\rm d}$ is the same as explained in Fig. 7. In Fig. 8(b), G_{yy} increases steeply with B near $B=2.4$ T due to the depopulation of the second sublevel and the sudden reduction of the DOS. The states near the bottom of $n=1$ sublevel carry little current due to their small group velocities, while contributing dramatically to the intersublevel elastic scattering rates for the electrons in the $n=0$ sublevel.

At very low temperatures $k_BT\ll\hbar\omega_{2k_{1F}}$, however, the B

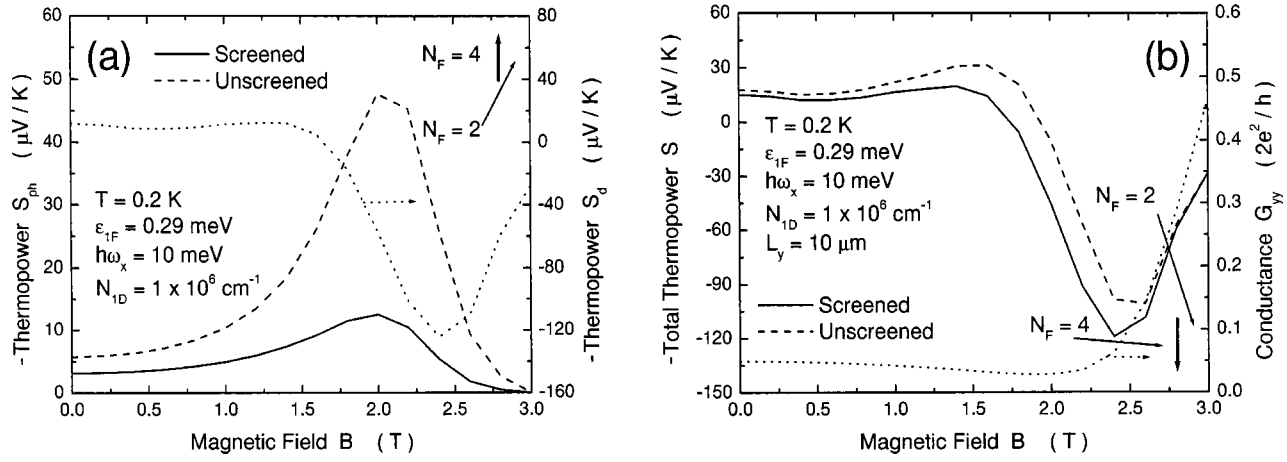

FIG. 9. B dependence of (a) $S_{\rm ph}$ (solid, dashed curves, left axis) and $S_{\rm d}$ (dotted curve, right axis) and (b) $S_{\rm ph}+S_{\rm d}$ (solid and dashed curves, left axis) and G_{yy} (dotted curve, right axis) at $T=0.2$ K for $\hbar\omega_x=10$ meV, $N_{1D}=1\times10^6$ cm^{-1}, and $L_y=10$ μm (for G_{yy}). Two sublevels are populated at $B=0$ with $\varepsilon_{1F}=0.29$ meV and $N_F=4$. Other parameters are given in the text.

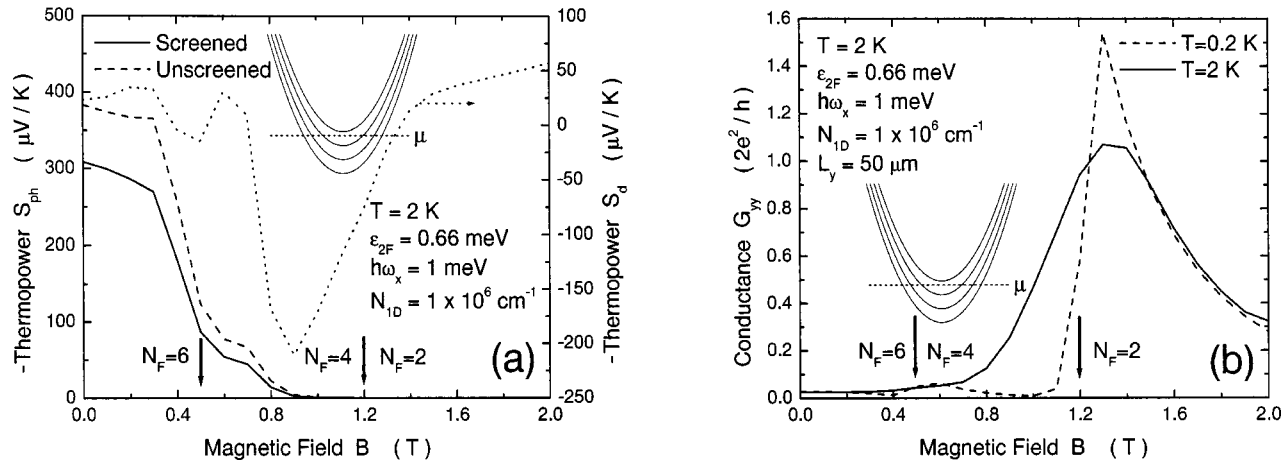

FIG. 10. B dependence of (a) $S_{\rm ph}$ (solid, dashed curves, left axis) and $S_{\rm d}$ (dotted curve, right axis) and (b) G_{yy} at $T=2$ K for $\hbar\omega_x=1$ meV, $N_{\rm 1D}=1\times10^6$ cm^{-1}, and $L_y=50$ μm (for G_{yy}). The third sublevel $n=2$ is populated at $B=0$ with $\varepsilon_{\rm 2F}=0.66$ meV (middle of the $n=2$ and $n=3$ sublevels) and $N_{\rm F}=6$. Other parameters are given in the text.

dependence of $S_{\rm ph}$ in Fig. 8(a) alters dramatically at low B as shown at 0.2 K in Fig. 9(a). In this case, $-S_{\rm ph}$ rises initially with B as in Fig. 4(a) due to $n_0(\omega_{s,\mathbf{q}})$ and DOS factors. However, the overlap factor $\Delta_{n'n}(q_x, q_y)$ becomes dominant at high B, decreasing $-S_{\rm ph}$ after a maximum. The depopulation effect is sharper in this case as seen for $-S_{\rm d}$. The minimum of $-S_{\rm d}$ is shifted to a slightly higher B compared with that in Fig. 8(a) because of a slightly larger value of μ at lower T. The conductance G_{yy} decreases with B initially as shown in Fig. 9(b) by a dotted curve (right axis) because of the increasing DOS around the thin thermal layer of μ but rises more steeply than in Fig. 8(b) when the $n=1$ sublevel is depopulated. The total thermopower $S_{\rm T}\equiv S_{\rm ph}+S_{\rm d}$ is displayed also in Fig. 9(b) by dashed and solid curves (left axis) and is positive above $B>1.7$ T. This large positive anomalous $S_{\rm T}$ is dominated by $S_{\rm d}$ and can be observed without being masked by $S_{\rm ph}$ in this regime.

At a much lower sublevel energy $\hbar\omega_x=1$ meV, the third sublevel $n=2$ is populated for $N_{\rm 1D}=1\times10^6$ cm^{-1}. Figure 10 shows $S_{\rm ph}$ (solid, dashed curves, left axis), $S_{\rm d}$ (dotted curve, right axis) in (a) at $T=2$ K and G_{yy} in (b) at $T=0.2$ and $T=2$ K as a function of B. The third sublevel Fermi energy $\varepsilon_{\rm 2F}=0.66$ meV at $B=0$ is near the middle between the levels $n=2$ and $n=3$. The magnitude of $S_{\rm ph}$ in (a) decreases initially with B due to the depopulation of the third sublevel at this high T as explained in Fig. 8(a), followed by a further monotonic reduction due to the B-induced suppression of $S_{\rm ph}$ through the overlap factor, and finally a complete suppression of $S_{\rm ph}$ for $B>1.0$ T. On the other hand, $S_{\rm d}$ displays quantum oscillations as a result of the two successive depopulations of sublevels and switches its sign around the depopulation B. In (b), G_{yy} decreases before the depopulation of the levels $n=3$ and $n=2$ at 0.2 K, rises and reaches maxima after the level depopulation. G_{yy} displays a sharp upward step near the depopulation of the second sublevel (second vertical arrow). At 2 K, however, the first maximum is smeared out, leaving only one large maximum near the second sublevel depopulation.

VII. CONCLUSIONS

We have examined the phonon-drag and electron-diffusion thermoelectric power at low temperatures as a function of temperature, magnetic field, and electron density, including the effect of multisublevel occupation. The electron conductance is dominated by elastic scattering in the temperature regime studied. The main role of the magnetic field is: (1) to monotonically increase the effective mass as well as the DOS along the wire thereby causing depopulation of the sublevels and quantum oscillations of the thermopower, and (2) to reduce the interaction and therefore the phonon-drag thermopower by displacing the electron wave functions of the initial and final states. Both the phonon-drag and the electron-diffusion contributions are found to exhibit unusual behavior unique to the one-dimensional system: In contrast to the well-known power-law (e.g., $\sim T^3$) behavior in higher dimensions, the phonon-drag thermopower decreases exponentially with decreasing temperature as $\propto\exp(-\hbar\omega_{\rm F}/k_BT)$ at low temperatures. Here $\hbar\omega_{\rm F}$ is approximately the phonon energy with the wave number $q_{\rm F}$ corresponding to the minimum momentum transfer for the back scattering. The electron-diffusion thermoelectric power becomes anomalous, namely positive, and is much larger in magnitude than the phonon-drag contribution when the chemical potential lies near the bottom of a sublevel (other than the ground sublevel) due to the presence of a strong one-dimensional van Hove singularity.

ACKNOWLEDGMENTS

Sandia is a multiprogram laboratory operated by Sandia Corporation, a Lockheed Martin Company, for the U.S. DOE under Contract No. DE-AC04-94AL85000.

[1] R. Fletcher, J. C. Mann, and G. Weimann, Phys. Rev. B **32**, 8477 (1985).
[2] R. Fletcher, M. D'Iorio, W. T. Moore, and R. Stoner, J. Phys. C **21**, 2681 (1988).
[3] M. Jonson and S. M. Girvin, Phys. Rev. B **29**, 1939 (1984).
[4] D. G. Cantrell and P. N. Butcher, J. Phys. C **19**, L429 (1986).
[5] S. K. Lyo, Phys. Rev. B **38**, 6345 (1988).
[6] S. K. Lyo, Phys. Rev. B **40**, 6458 (1989).
[7] S. S. Kubakaddi, P. N. Butcher, and B. G. Mulimani, Phys. Rev. B **40**, 1377 (1989).
[8] S. S. Kubakaddi and P. N. Butcher, J. Phys.: Condens. Matter **1**, 3939 (1989).
[9] M. Tsaousidou and P. N. Butcher, Phys. Rev. B **56**, R10 044 (1997).
[10] S. K. Lyo and D. Huang, Phys. Rev. B **64**, 115320 (2001).
[11] H. Akira and T. Ando, Phys. Rev. B **43**, 11 676 (1991).
[12] K.-F. Berggren, G. Roos, and H. van Honten, Phys. Rev. B **37**, 10 118 (1988).
[13] J. M. Ziman, *Electrons and Phonons*, p. 298 (Oxford University Press, London, 1967); J. M. Ziman, *Principles of the Theory of Solids*, pp. 212–215 (Cambridge Press, Second edition, 1972).
[14] M. Bailyn, Phys. Rev. **157**, 480 (1967).
[15] J. L. Opsal, in *Thermoelectricity in Metallic Conductors*, Eds. F. Blatt and P. A. Schroeder, p. 241 (Plenum Press, New York, 1978).
[16] S. K. Lyo, Phys. Rev. B **43**, 2412 (1991).
[17] M. N. Wybourne, C. G. Eddison, and M. J. Kelly, J. Phys. C **17**, L607 (1984).
[18] J. D. Zook, Phys. Rev. A **136**, 869 (1964).
[19] K. Esfarjani, H. R. Glyde, and V. Sa-yaknit, Phys. Rev. B **41**, 1042 (1990).
[20] D. Huang and M. O. Manasreh, Phys. Rev. B **54**, 5620 (1996).
[21] G. Fishman, Phys. Rev. B **34**, 2394 (1986).
[22] S. Das Sarma and W. Lai, Phys. Rev. B **32**, 1401 (1985).
[23] R. Fletcher, J. J. Harris, and C. T. Foxon, Semicond. Sci. Technol. **v6**, 54-58 (1991).